The Establishment of Intervertebral Endplate Degeneration: A Novel in-vivo Diurnal-Axial Controllable Loading Model in Rat Tail

Zhouyang Hu
Shanghai East Hospital, Tongji University School of Medicine https://orcid.org/0000-0003-1535-3952
Fan He
Shanghai East Hospital
Xinhua Li
Shanghai East Hospital
Bei Jiang
Shanghai East Hospital
Shuaifeng Yan
Shanghai East Hospital
Jun Tan
Shanghai East Hospital
Mingjie Yang
Shanghai East Hospital
Lijun Li (orthopedics123@qq.com)
https://orcid.org/0000-0002-4595-2908

Research article

Keywords: cartilage endplate degeneration, animal model, axial loading, controllable loading, Schmorl's node

Posted Date: May 22nd, 2020

DOI: https://doi.org/10.21203/rs.3.rs-29923/v1

Abstract

Background. Cartilage endplate (CEP) acts as an important mechanical barrier and nutrient channel for the intervertebral disc (IVD). Its vulnerability to excessive loading and subsequent degeneration might be an initial trigger for IVD degeneration. This study aims to build a new in-vivo animal model of rat-tail CEP degeneration through implementing a controllable axial compressive device.

Methods. An axial controllable compressive load was conducted on the 8–9 th coccygeal IVD of adult rat tail through puncturing 4 Kirschner wires into its superior and inferior vertebra. The exact compression loads were controlled and adjusted by a remote controller. The compression and decompression periods were set as 8 h/16 h per day. The control group was set as no device installation, while the Kirschner wires were punctured without compression in the sham group. After each 4, 8 and 12 weeks, 3 rats in each group were sacrificed and compressed disc were analyzed.

Results. After compression, the targeted CEP degenerated gradually with time. Through 12 weeks' loading, the CEP structure collapsed completely and the Schmorl's nodes formed and penetrated from the cartilage layer into the vertebra. When compared with the control group, the number of micro porosities in the CEP becomes extremely scarce with loading, while the content of aggrecan and collagen II decreased significantly. However, these significant changes did not show up when sham and control groups were compared.

Conclusions. A new excessive force induced CEP degeneration animal model was developed with its contribution as a practical alternative for further studying mechanisms of CEP degeneration.

Background

The cartilage endplate (CEP) is an important component of the intervertebral disc tissue. It is a cartilage-like tissue that connects the upper and lower vertebral bodies with the annulus fibrosus (AF) and nucleus pulposus. As one of the biomechanical barriers, the superior and inferior CEP can absorb and disperse various forms of mechanical forces. The special micro-porous structure of the CEP tissue serves as one of the most important channels for supplying nutrition from vertebrae to the gel-like nucleus pulposus (NP) [1]. Once the endplate is degenerated, the abnormal changes such as disrupted nutrition supply and atypical intramedullary pressure to the cellular microenvironment within the structures of the disc cells would finally lead to tissue breakdown and functional impairments [2, 3].

Although human intervertebral disc (IVD) is susceptible to various forms of forces, axial load plays an important role in the pathogenesis of its degeneration [4, 5]. Some studies believed that the cartilaginous endplate is the weakest point under the compression of axial force and the excessive damage caused by it acting as the initiating factor of IVD degeneration [6]. Therefore, to establish an axial force-induced animal model of CEP degeneration and observe its morphological changes during the process of degeneration is critically important.

In the past, many helpful efforts have been made for building an effective animal models of CEP degeneration, such as osteoporosis modeling, autoimmune response and chemicals injection [7–9], yet *in vivo* biomechanical approach have not been considered in these studies. Despite these, in animal models of IVD (*mainly on NP*), biomechanical apparatus as ilizarov-type external fixator was applied by many studies [10–12]. Moreover, it is widely modified for use in the field of orthopedic surgery in order to correct bone deformities. However, the disadvantages of this apparatus are also prominent such as unchanged loading module and imprecise compressive forces during long-term experiment. Most importantly, according to our knowledge, its function as inducing CEP degeneration has not been studied. Therefore, in the current study we designed a novel and reliable model for causing CEP degeneration on rat tail IVD. By means of penetrating four Kirschner wires into two adjacent vertebrae, this custom-build compressive device with controllable loading module was applied to the rat tail. Our aim of this study was to use this device for providing stable axial compressive forces in long term and to observe the effects of these forces to the pathological changes of CEP during different phases of degeneration.

Methods

Ethical Approval and Animal Grouping

The experimental protocols were reviewed and approved by the Ethics Committee on Animal Studies of Shanghai East Hospital, Tongji University School of Medicine. Animal welfare was assessed and guided strictly following the guideline in Research Animal welfare of Shanghai East Hospital. Thirty three-months-old male Sprague-Dawley rats (SD) were used in this study (SLAC Laboratory Animal Co., Ltd, Shanghai, China). All rats were group-housed in standard plastic cages by 3 per cage and raised in the specific pathogen-free (SPF) laboratory of Shanghai east hospital. A total of twenty seven rats were randomly assigned into three groups: the operational Group A applied with compressive device (n = 9), the Sham Group B carrying devices without compression (n = 9), and the control Group C (n = 9), respectively. Three rats were randomly chosen for sacrifice in each group at time frames (4, 8 and 12 weeks).

Establishment Of The Compression Device

The custom-made device consists of three main parts (Fig. 1). 1) For the compressive unit, one geared motor equipped with screw rod were penetrated through three aluminum rings (with four drilled holes); one pressure sensor was inserted in between two aluminum rings (Fig. 1a, b). 2) The control box that connects the compressive unit through wire provides one screen which shows the compressive force, one signal receiving unit and one power bank that connects to the above two units for electrical energy (inside of the box), as shown in Fig. 1c. 3) An infrared remote controller was provided for increasing or decreasing compressive force, as shown in Fig. 1d.

Surgical Procedures

As shown in Fig. 2, the model was both installed in the tail of SD rats in operation group A and the sham group B. Animals were anesthetized with the injection of 4% chloral hydrate (0.1 ml/kg body wt, Sangon Biotech, Shanghai, China) by means of intra-peritoneal local anesthesia (Fig. 2a).). The prone position was taken for the operation. First, the compressive unit was penetrated through the tail. Four Kirschner wires (0.9 mm) were respectively inserted into the center of 8th and 9th coccygeal vertebrae (Co 8/9) through two aluminum rings. Then an instruction of increasing force was taken by pressing the button on the infrared remote controller in order to press the disc between Co 8 and 9. As previous studies described [10, 13], 1.3 MPa compressive stress was installed to the targeted disc. The diameters and area of Co 8/9 disc was measured and calculated using a Vernier caliper tightened to the skin of Co 8/9 disc (Fig. 2b). Then the force value that needed to be conducted was calculated according to pressure-force-area formula. The force value in Newton (N) can be displayed in real time on the screen of the control box, therefore an increased compression command was continuously given to the control box until the pre-determined force value was reached (Fig. 2c). The loading duration was set as 8-hours loading and 16-hours free loads in one single day [14]. A protection of shield was then installed around the compressive unit in case of rat-biting damage to the connecting wires. For rats in sham operation group B, force compression command was not performed after the puncture of Kirschner wires. Amoxicillin trihydrate subcutaneous injection (7 mg/kg body wt, Yuanye Bio-Technology Co., Ltd, Shanghai, China) was used to prevent infection within one week after the surgery. Pain killer analgesic ibuprofen granules (5 mg/kg body wt, HPGC, Harbin, China) for one week were used by intragastric administration.

Mri Examinations

After 4, 8 and 12 weeks of the operation, the Co 8/9 disc of each 3 rats in Group A, B and C were respectively sacrificed for magnetic resonance imaging (MRI) examination. A MRI scanner (Achieva 3.0T; Philips Medical Systems, Best, the Netherlands) was used with the following parameters: T1-weighted imaging: TR = 300 ms, TE = 20 ms, FOV = 60mm × 60 mm, data matrix = 148 × 150, and slice thickness = 1 mm. T2-weighted imaging: TR = 5000 ms, TE = 50 ms, FOV = 60 mm × 60 mm, data matrix = 200 × 200, and slice thickness = 1 mm. Two senior radiologists independently read and assessed the MRI image results. The degree of IVD was assessed using the Pfirrmann grading classification system [15].

Formalin-fixed Paraffin-embedded Tissue Preparation

After 4, 8 and 12 weeks of axial compression, the rats were sacrificed by fixation procedure using 4% paraformaldehyde perfused via the circulation system [16]. The targeted disc unit (Co8/9) was extracted and fixed in 4% paraformaldehyde, decalcified in 10% 0.5M ethylenediaminetetraacetic acid (EDTA) (Servicebio Co., Ltd, Wuhan, China) and then embedded in EM-400 embedding medium paraffin. Disc tissues were sectioned at 5 μm thickness using a microtome (Leica RM2235, Biosystems, Wetzlar, Germany).

Histological Evaluations

The disc sections were stained with hematoxylin and eosin (HE) and Safranin-O Fast Green (SOFG) and analyzed qualitatively to observe the morphological changes of degenerated cartilage endplates using a microscope (Leica DM6000B, Microsystems, Wetzlar, Germany). A histological classification system was used to assess the characteristics of degeneration [17].

Immunohistochemistrical Staining

Matrix collagen II and collagen II were performed as markers of endplate and IVD degeneration. The immunohistochemical staining was performed using the following primary antibodies: mouse monoclonal collagen II antibody (1:150, ab185430, Abcam, Cambridge, UK); mouse monoclonal collagen II antibody (1:150 dilution, ab3773, Abcam, Cambridge, UK). For detection, 3, 30-diaminobenzidine was used; positive cells were stained brown. Nuclei were counter-stained blue with hematoxylin. All stained preparations were photographed under a microscope (Leica DM6000B, Microsystems, Wetzlar, Germany). Then the stained sections were semi-quantitatively analyzed by means of Image-Pro Plus 7.0 software (Media Cybernetics, Inc., Rockville, USA). The average optical density was measured on the images at 400 × magnification.

Statistical analysis

Two-tailed Student *t*-test was performed using SPSS 20.0 version (IBM Inc., Chicago, IL, USA). The experiment data were presented as mean ± standard deviation (SD). The level of statistical significance was set at $P < 0.05$.

Results

Animals

There are in total 27 rats were included in this study. However, after the loading operation, there is one rat in Group A failed to carry the loading device due to the ischemic necrosis of tail. In Group B, one rat died of the anesthesia intolerance during the device installing operation.

Mri Results

In the operational group, after continuous loading, the signal of Co8/9 disc decreased significantly (Fig. 3A). In the sham operation group, the Co8/9 vertebral Kirschner wire penetration marks were observed, showing a low signal; no significant signal changes of the loaded discs at 4, 8, and 12 weeks after loading were observed (Fig. 3B). In the control group, however, the T2 images of the Co 8/9 intervertebral disc showed high signal during the whole experimental process; The boundary between CEP

and NP was clear and the intervertebral space height was normal (Fig. 3C). Table 1 shows the grading scores of loaded disc in three different groups.

Table 1
The grading scores of Co8/9 in three different groups, showing with five levels and equivalent number.

Pfirrmann grading scores			
Operation duration (weeks)	4	8	12
Group A	II = 1	III = 1	V = 2
	III = 6	IV = 3	
	IV = 1	V = 1	
Group B	I = 7	I = 4	I = 1
	II = 1	II = 1	II = 1
Group C	I = 9	I = 6	I = 3

He & Sofg Staining And Scoring Results

In the control group, the gross structure and thickness of CEP was complete and uniform; The distribution of micro-porosity with regular size can be observed. The NP cells were rounded like and there was no sign of no cell cluster or fibrosis. The AF ring has a well-organized and lamellar architecture. The boundaries between CEP, NP and AF were well-defined (shown in Fig. 4, 5 control group a1-a4).

In the sham surgery group, the structure of CEP was also normal and complete. However, the appearance of a curved AF structure was observed. The SOFG histological scores after 4-12weeks' loading were 0.4 ± 0.8, 0.7 ± 0.6, and 1.1 ± 0.5, respectively (Table 2).

Table 2
The SOFG histological grading scores of Co8/9 disc in three groups (+ S).

	4weeks	8weeks	12weeks
Group A	5.4 ± 2.1*	7.6 ± 2.5*	11.3 ± 1.2*
Group B	0.4 ± 0.8	0.7 ± 0.6	1.1 ± 0.5
Group C	0	0	0
* indicates the statistical differences compared to Group B (P = 0.02, 0.01 and 0.00, respectively)			

In the experimental group: 1) after 4weeks' loading, in the degenerated CEP, there were more inflammatory cells accumulating inside of the micro-porosity region. At the same time, the diameter of the micro-porosity increased (c1/c3 in Figs. 4 and 5); the size and the water content of the NP decreased (c1/c4 in Figs. 4 and 5). The AF was compressed into an S-type cycle under loading (c2 in Figs. 4 and 5). The SOFG histological score was 5.4 ± 2.1 on average (Table 2); 2) After 8 weeks' loading, a significant thinned CEP was shown. The number of micro-porosities in CEP decreased and its structure became irregular. The calcified NP ruptured through the superior and inferior endplates (Schmorl's node) as shown in d1/d4 of Fig. 4, 5; The AF was severely ruptured and disordered. The SOFG histological score averaged 7.6 ± 2.5 (Table 2). 3) After 12weeks' loading, the micro-porosities in the CEP almost disappeared, and the structure of CEP was severely broken. The notochordal cells almost disappeared, and a large amount of cartilage fibrosis and calcification occurred in the central region. More NP tissues penetrated into the vertebral area, and AF was severely ruptured and disordered (e1-e4 in Fig. 4, 5). The SOFG histological score averaged as 11.3 ± 1.2 (Table 2).

Immunohistochemistrical results

For the aggrecan expressions in CEP and NP, they dropped dramatically after the abnormal mechanical loading was applied to. After 4- and 8-weeks' compression, the complete tissues structure collapsed and enlarged NP and CEP cells expressed very limited aggrecan (Fig. 6c-e and Fig. 8). However, there are no significant differences of aggrecan expressions in both NP and CEP when the control and the sham groups were compared, respectively (Fig. 6a, b and Fig. 8).

In the control group and the sham-operated group, the collagen II contents in the CEP and NP were rich and concentrated (as shown in Fig. 7a, b), and there were no statistical expression differences between the two groups. After 4–8 weeks' loading, this matrix gradually fragmented and dispersed, and its content decreased significantly in NP but not obviously in CEP. Fibroblast-like cells shown in the NP area (Fig. 7c, d). After 12 weeks' loading, both in the structure of NP and CEP, the positive stainings were severely reduced (Fig. 7e). As shown in Figs. 7 and 8, when comparing the expression of matrix collagen II in CEP and NP between the control and the loading group in each time point, the differences were statistically significant. ($P < 0.05$).

Discussion

Although the CEP tissue plays an important role in IVD, it has not been extensively studied compared with NP, possibly because the tissue layer is so thin rendering it difficult to harvest [18]. However, the structural failure always started in the endplate, indicating that these thin cartilage layers are the weak parts susceptible to excessive mechanical loading [19, 20]. In this study, with the aim of inducing CEP degeneration, we established a novel diurnal-axial loading device based on Ilizarov-type apparatus and applied it to rat tail *in vivo.*

This device was developed in order to provide a stable and precise axial loading force. The loading force created by the compressive unit would drive the motion of two aluminum rings on the coccygeal of rat tail. The Kirschner wires that penetrated the two adjacent vertebrae through aluminum rings were driven close to each other. The targeted disc was then compressed with pre-set force that can be precisely adjusted following the monitor. Meanwhile, in order to test the penetrating effects of wires to the vertebra and the following potential effect to CEP, the sham operational group was set and examined. No significant signs of CEP degeneration were found in the sham group, suggesting the little effect of wire punctuation to the cause of CEP degeneration. There are many loading devices built for inducing cartilage degeneration. One rat tail bending model was established by Lindblom et al. [21]. They found that disc on the concave curved side degenerated significantly with direct damage to the tissue structure and cell number. Further, the degree of degeneration heavily depends on time and the extent of bending force applied to the rat tail. Another classic model, Ilizarov-type compressive model, was widely used by many researchers due to its reliable installation and satisfactory modeling results [11, 22–24]. However, a set of *springs* were mainly used in these studies as the provider of compression loads. A stable and reliable compressive effect cannot last long due to the *spring fatigue*. Meanwhile, the *static* loading mode is not comparable to the physiological mechanical loading conditions of CEP during daily activities.

In our study, after loading, the targeted Co8/9 disc degenerated with time. The histological staining scores were 5.4 ± 2.1, 7.6 ± 2.5 and 11.3 ± 1.2 after 4, 8 and 12 weeks, respectively. The loaded disc showed the sign of severe and significant degeneration: the NP was severely dehydrated and fibrotic, while the number of intervertebral cells were largely decreased. The micro-porosities in CEP disappeared during the phase of degeneration. Under loading, the degenerated discs ruptured through the cracked CEP with the formation of Schmorl's nodules. Kuga et al. [25] found in a fatigue stress test of spinal functional units investigate that the AF is prone to rupture; and the CEP is a weak area that susceptible to repetitive motion stress. Zehra et al. [26] found that abnormal pressure loading can cause the failure of CEP showing that the CEP is thinning with degeneration. They also found that the degree of IVD is strongly associated with multi and large CEP defects, which might contribute to the volume and compression change inside the NP [27]. Maclean JJ et al. [28] observed the effects of short-term high-force compressive loading to the rat intervertebral disc by means of Ilizarov-type device. Their findings show that abnormal compression can cause a decreased expression of collagen I and II and an increase d expression of catabolic genes such as collagen IIase-1 etc., which may lead to the breakdown of collagen II, a significant key extracellular matrix in the intervertebral disc.

With the progression of degeneration, the extracellular matrix collagen II and collagen II gradually disappear. Immunohistochemical stainings showed when comparing with the control group, the expression of collagen II in NP of the experimental group was reduced by 39.8%, 65.4% and 80.7% at 4W, 8W, 12 weeks after the operation; and were 22.5%. 56.2% and 71.3% in CEP; For collagen II, the expression in the experimental group were reduced by 42.6%, 57.9% and 73.4%, after the operation; were 48.6%, 74.8% and 86.5% in CEP, respectively. At the same time, there was no significant difference in the expression of the aggrecan and collagen II in the Co8/9 disc of sham operation group compared with the control group (P = 0.36). Since the modeling procedure acquired the penetration of vertebral body, whether

the nutritional disorder would be a confounding factor which affecting the results is also the focus of this experiment. Studies found that high-force loading could cause intracellular environmental disorders, the activation of inflammatory factors and the production of matrix metalloproteinases, in the end, leading to the continuous decomposition and destruction of extracellular matrix. Yamazaki et al. [29] proposed that abnormal pressure load would up-regulate the catabolism related factors and induce the expression increase of matrix degrading and proteolytic enzyme. Ariga et al. [30] conducted an ex vivo study and observed increased number of apoptotic CEP cells with increased static mechanical loading force.

There are several limitations in the current study. First of all, from the perspective of physiological characteristics. This model simply takes the axial compression load into consideration, while the realistic biomechanics of the human intervertebral disc are more complicated. Based on our knowledge there is no *in-vivo* study which simulates the effects of comprehensive mechanical effects such as torsion and shear force to the CEP [31]. Second, the applied loading force and loading frequency of the model are manually controlled in a diurnally setting mode yet cannot mimic the physiological loading condition of the human spine. Thirdly, rat was selected in our experiment as the model. Compared with large animals, the extracellular matrix of the IVD in small animal like rat contains higher water content and the existence of notochordal cells in its disc made the results hard to be comparable with human discs. In the future, a compressive device with multi-frequencies and loading settings controlled by a wireless terminal should be developed. Further, large animal models such as goat, cattle and even ape with similar spine biomechanical backgrounds are to be considered.

Conclusion

We successfully established a new animal model of CEP degeneration induced by excessive axial force using rat tail. This model could serve as a useful tool for further etiological and pathophysiological study of CEP degeneration mechanisms.

Abbreviations

CEP
Cartilage Endplate
AF
Annulus Fibrosus
IVD
Intervertebral Disc
NP
Nucleus Pulposus
SPF
Specific Pathogen Free
SD
Sprague Dawley

MRI
Magnetic Resonance Imaging
N
Newton (Unit)
EDTA
Ethylenediaminetetraacetic Acid
HE
Hematoxylin and Eosin
SOFG
Safranin-O Fast Green
SD
Standard Deviation

Declarations

Ethics approval and consent to participate

The experimental protocols were reviewed and approved by the Ethics Committee on Animal Studies of Shanghai East Hospital, Tongji University School of Medicine.

Consent for publication

Not applicable.

Availability of data and materials

All data generated or analyzed during this study are included in this published article.

Competing interests

We declare there is no competing interest.

Funding

This work were funded by the Key Discipline Construction Project of Pudong Health Bureau of Shanghai, No. PWZxk2017-08; Natural Science Foundation of Jiangxi Province, No. 20171BAB205034; Scientific Project of Shanghai Municipal Health & Family Planning Commission, No. 201640063.

Authors contribution

ZYH: designed the study, performed the HE & SOFG Staining, built the animal model and drafted the paper.

FH, helped perform the MRI, immunohistochemical work and build the animal model.

XHL, collected the immunohistochemical & histochemical data and revised the paper.

BJ: helped perform the MRI and the manage animal work.

SFY, collected and analyzed MRI data.

JT, interpreted data and revised the paper.

MJY, interpreted data, made the figures and finalized the paper.

LJL, designed and funded the study, revised and finalized the paper.

Acknowledgements

We would like also to thank for the model technology providing and device producing from Shanghai Preclinic Medical Technology Co., Ltd.

References

1. DeLucca JF, Cortes DH, Jacobs NT, Vresilovic EJ, Duncan RL, Elliott DM. Human cartilage endplate permeability varies with degeneration and intervertebral disc site. Journal of biomechanics. 2016;49(4):550–7.
2. Yuan FL, Zhao MD, Jiang DL, Jin C, Liu HF, Xu MH, et al. Involvement of acid-sensing ion channel 1a in matrix metabolism of endplate chondrocytes under extracellular acidic conditions through NF-kappaB transcriptional activity. Cell stress chaperones. 2016;21(1):97–104.
3. Kang R, Li H, Ringgaard S, Rickers K, Sun H, Chen M, et al. Interference in the endplate nutritional pathway causes intervertebral disc degeneration in an immature porcine model. International orthopaedics. 2014;38(5):1011–7.
4. Adams MA, Freeman BJ, Morrison HP, Nelson IW, Dolan P. Mechanical initiation of intervertebral disc degeneration. Spine. 2000;25(13):1625–36.
5. Vergroesen PP, Kingma I, Emanuel KS, Hoogendoorn RJ, Welting TJ, van Royen BJ, et al. Mechanics and biology in intervertebral disc degeneration: a vicious circle. Osteoarthritis cartilage. 2015;23(7):1057–70.
6. Rade M, Määttä JH, Freidin MB, Airaksinen O, Karppinen J, Williams FMK. Vertebral Endplate Defect as Initiating Factor in Intervertebral Disc Degeneration: Strong Association Between Endplate Defect and Disc Degeneration in the General Population. Spine. 2018;43(6):412–9.
7. Zhong R, Wei F, Wang L, Cui S, Chen N, Liu S, et al. The effects of intervertebral disc degeneration combined with osteoporosis on vascularization and microarchitecture of the endplate in rhesus monkeys. European spine journal: official publication of the European Spine Society, the European Spinal Deformity Society, and the European Section of the Cervical. Spine Research Society. 2016;25(9):2705–15.

8. Han C, Wang T, Jiang HQ, Ma JX, Tian P, Zang JC, et al. An Animal Model of Modic Changes by Embedding Autogenous Nucleus Pulposus inside Subchondral Bone of Lumbar Vertebrae. Scientific reports. 2016;6:35102.
9. Yuan W, Che W, Jiang YQ, Yuan FL, Wang HR, Zheng GL, et al. Establishment of intervertebral disc degeneration model induced by ischemic sub-endplate in rat tail. The spine journal: official journal of the North American Spine Society. 2015;15(5):1050–9.
10. Iatridis JC, Mente PL, Stokes IA, Aronsson DD, Alini M. Compression-induced changes in intervertebral disc properties in a rat tail model. Spine. 1999;24(10):996–1002.
11. Hirata H, Yurube T, Kakutani K, Maeno K, Takada T, Yamamoto J, et al. A rat tail temporary static compression model reproduces different stages of intervertebral disc degeneration with decreased notochordal cell phenotype. Journal of orthopaedic research: official publication of the Orthopaedic Research Society. 2014;32(3):455–63.
12. Xia W, Zhang LL, Mo J, Zhang W, Li HT, Luo ZP, et al. Effect of Static Compression Loads on Intervertebral Disc: An in Vivo Bent Rat Tail Model. Orthopaedic surgery. 2018;10(2):134–43.
13. Lotz JC, Colliou OK, Chin JR, Duncan NA, Liebenberg E. Compression-induced degeneration of the intervertebral disc: an in vivo mouse model and finite-element study. Spine. 1998;23(23):2493–506.
14. Korecki CL, MacLean JJ, Iatridis JC. Characterization of an in vitro intervertebral disc organ culture system. European spine journal: official publication of the European Spine Society, the European Spinal Deformity Society, and the European Section of the Cervical. Spine Research Society. 2007;16(7):1029–37.
15. Pfirrmann CW, Metzdorf A, Zanetti M, Hodler J, Boos N. Magnetic resonance classification of lumbar intervertebral disc degeneration. Spine. 2001;26(17):1873–8.
16. Gage GJ, Kipke DR, Shain W. Whole animal perfusion fixation for rodents. Journal of visualized experiments: JoVE. 2012(65).
17. Rutges JP, Duit RA, Kummer JA, Bekkers JE, Oner FC, Castelein RM, et al. A validated new histological classification for intervertebral disc degeneration. Osteoarthritis cartilage. 2013;21(12):2039–47.
18. Natarajan RN, Ke JH, Andersson GB. A model to study the disc degeneration process. Spine. 1994;19(3):259–65.
19. Brinckmann P, Frobin W, Hierholzer E, Horst M. Deformation of the vertebral end-plate under axial loading of the spine. Spine. 1983;8(8):851–6.
20. Herrero CF, Garcia SB, Garcia LV, Aparecido Defino HL. Endplates changes related to age and vertebral segment. BioMed research international. 2014;2014:545017.
21. Lindblom K. Intervertebral-disc degeneration considered as a pressure atrophy. J Bone Joint Surg Am. 1957;39-a(4):933 – 45.
22. Yan Z, Pan Y, Wang S, Cheng M, Kong H, Sun C, et al. Static Compression Induces ECM Remodeling and Integrin α2β1 Expression and Signaling in a Rat Tail Caudal Intervertebral Disc Degeneration Model. Spine. 2017;42(8):E448-e58.

23. Vasiliadis ES, Kaspiris A, Grivas TB, Khaldi L, Lamprou M, Pneumaticos SG, et al. Expression of macrophage elastase (MMP12) in rat tail intervertebral disc and growth plate after asymmetric loading. Bone joint research. 2014;3(9):273–9.
24. Terashima Y, Kakutani K, Yurube T, Takada T, Maeno K, Hirata H, et al. Expression of adiponectin receptors in human and rat intervertebral disc cells and changes in receptor expression during disc degeneration using a rat tail temporary static compression model. J Orthop Surg Res. 2016;11(1):147.
25. Kuga N, Kawabuchi M. Histology of intervertebral disc protrusion: an experimental study using an aged rat model. Spine. 2001;26(17):E379-84.
26. Zehra U, Robson-Brown K, Adams MA, Dolan P. Porosity and Thickness of the Vertebral Endplate Depend on Local Mechanical Loading. Spine. 2015;40(15):1173–80.
27. Zehra U, Flower L, Robson-Brown K, Adams MA, Dolan P. Defects of the vertebral end plate: implications for disc degeneration depend on size. The spine journal: official journal of the North American Spine Society. 2017;17(5):727–37.
28. MacLean JJ, Lee CR, Grad S, Ito K, Alini M, Iatridis JC. Effects of immobilization and dynamic compression on intervertebral disc cell gene expression in vivo. Spine. 2003;28(10):973–81.
29. Yamazaki S, Banes AJ, Weinhold PS, Tsuzaki M, Kawakami M, Minchew JT. Vibratory loading decreases extracellular matrix and matrix metalloproteinase gene expression in rabbit annulus cells. The spine journal: official journal of the North American Spine Society. 2002;2(6):415–20.
30. Ariga K, Yonenobu K, Nakase T, Hosono N, Okuda S, Meng W, et al. Mechanical stress-induced apoptosis of endplate chondrocytes in organ-cultured mouse intervertebral discs: an ex vivo study. Spine. 2003;28(14):1528–33.
31. Newell N, Little JP, Christou A, Adams MA, Adam CJ, Masouros SD. Biomechanics of the human intervertebral disc: A review of testing techniques and results. J Mech Behav Biomed Mater. 2017;69:420–34.

Figures

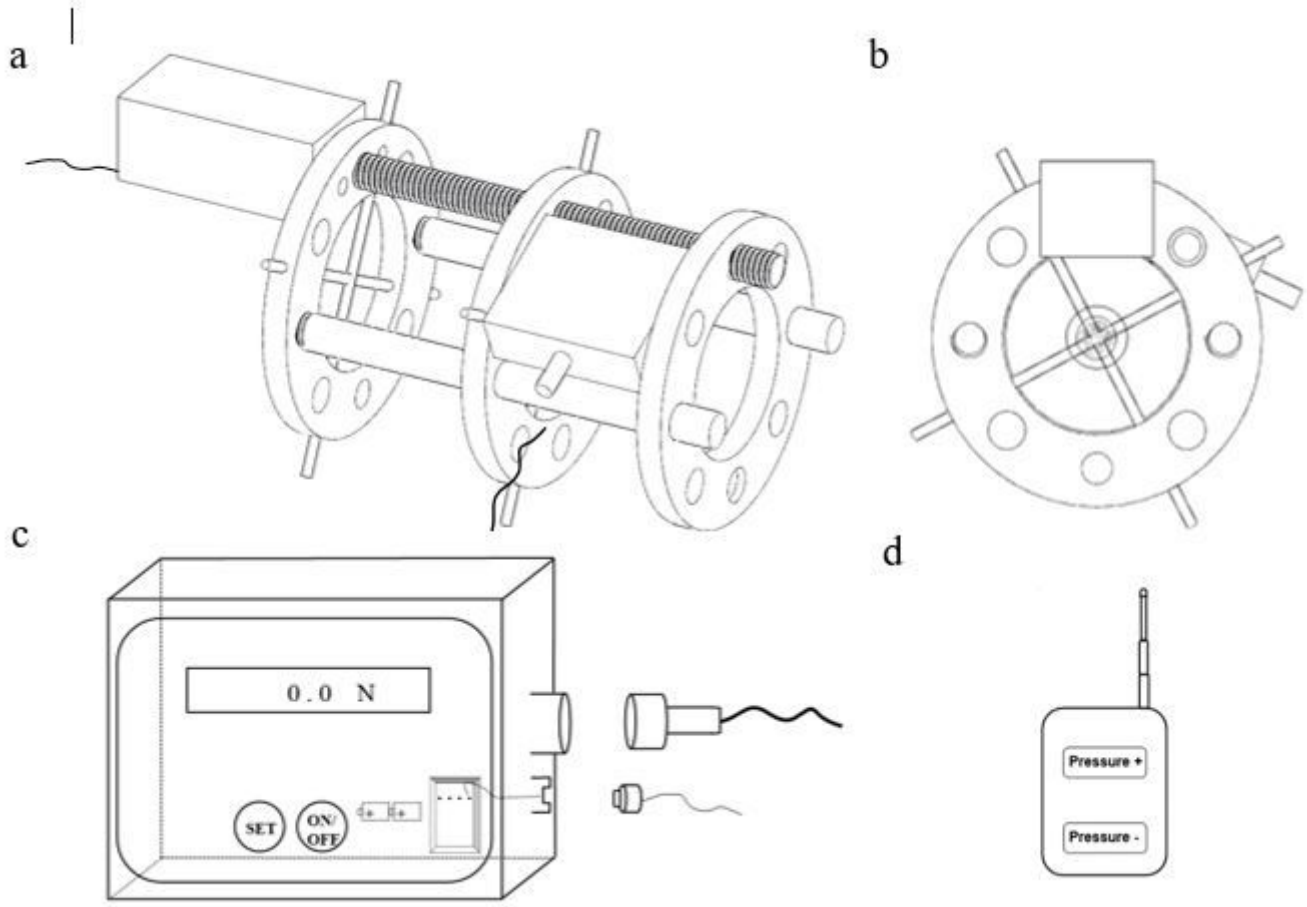

Figure 1

Constructive schematic of the custom-build compressive loading device. The compressive unit with a. frontal view; b. axial view; c. the control box with signal receiver and power bank; d. the infrared remote controller.

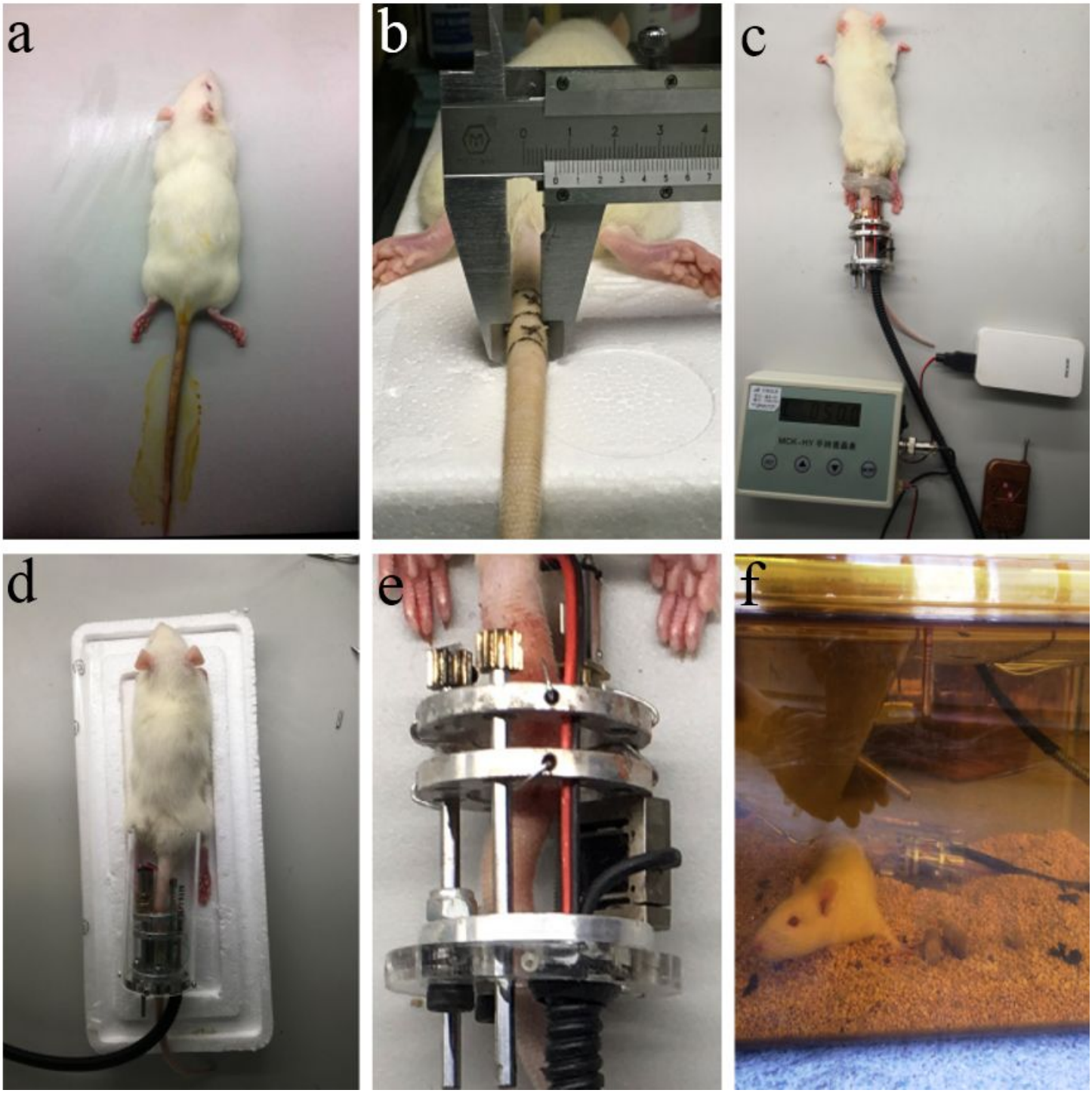

Figure 2

The schematic of installation. a. tail disinfection; b. diameter measurement of the Co 8/9 disc by a caliper; c. the compressive force adjustment to the per-determined value; d. installation of a protective shield; e. disinfection after the operation; f. the living status of the mouse after operations.

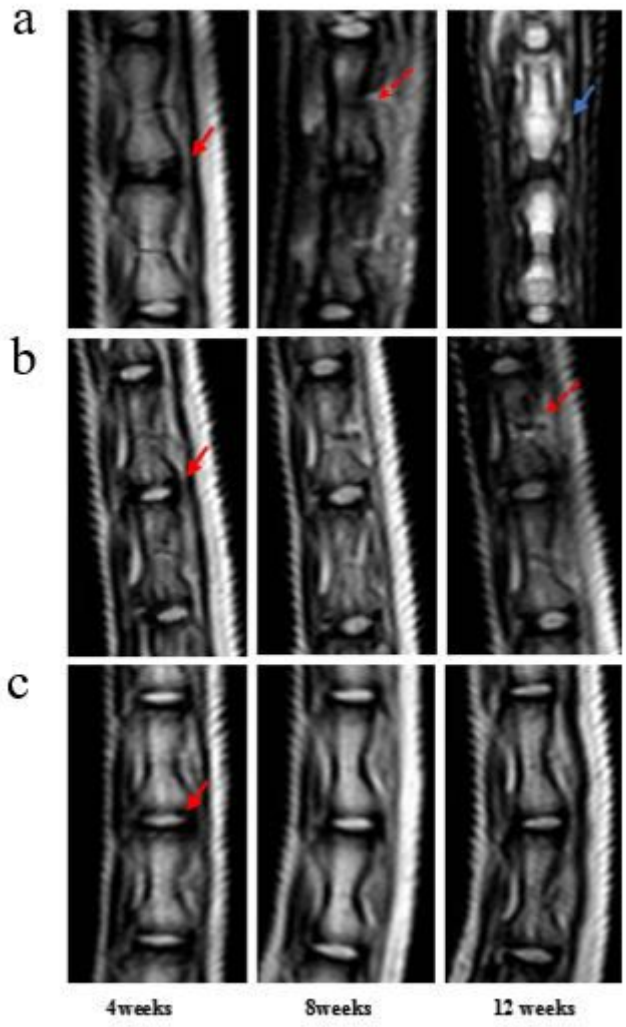

Figure 3

MRI T2 images of loaded Co8-9 intervertebral disc (as shown with solid red arrows) in the a. operational group, b. sham group and c. control group after 4, 8 and 12 weeks of operation. The red dotted arrows indicate the punctured passages; the blue solid arrow shows the sign of osteosclerosis.

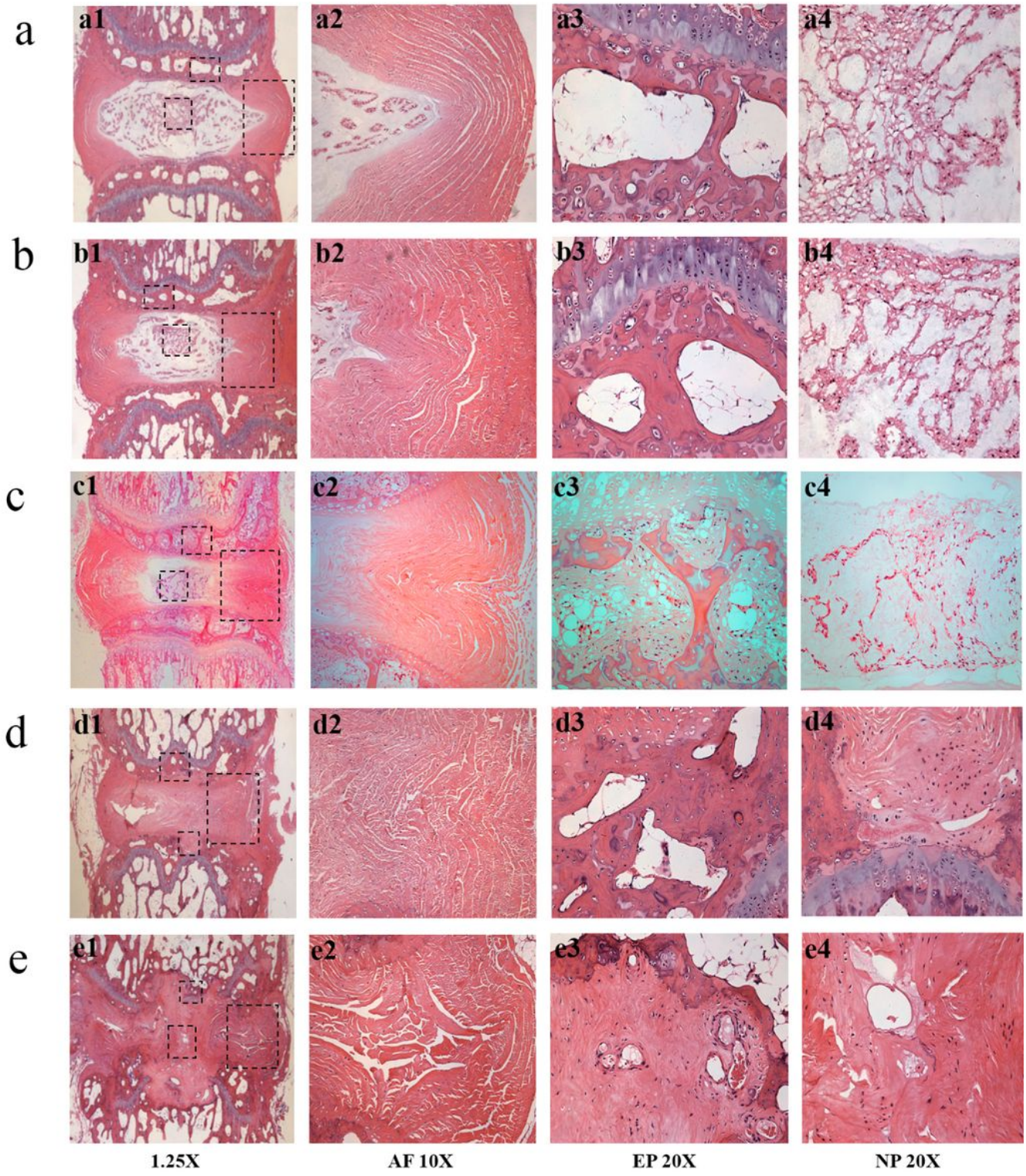

Figure 4

MRI T2 images of loaded Co8-9 intervertebral disc (as shown with solid red arrows) in the a. operational group, b. sham group and c. control group after 4, 8 and 12 weeks of operation. The red dotted arrows indicate the punctured passages; the blue solid arrow shows the sign of osteosclerosis.

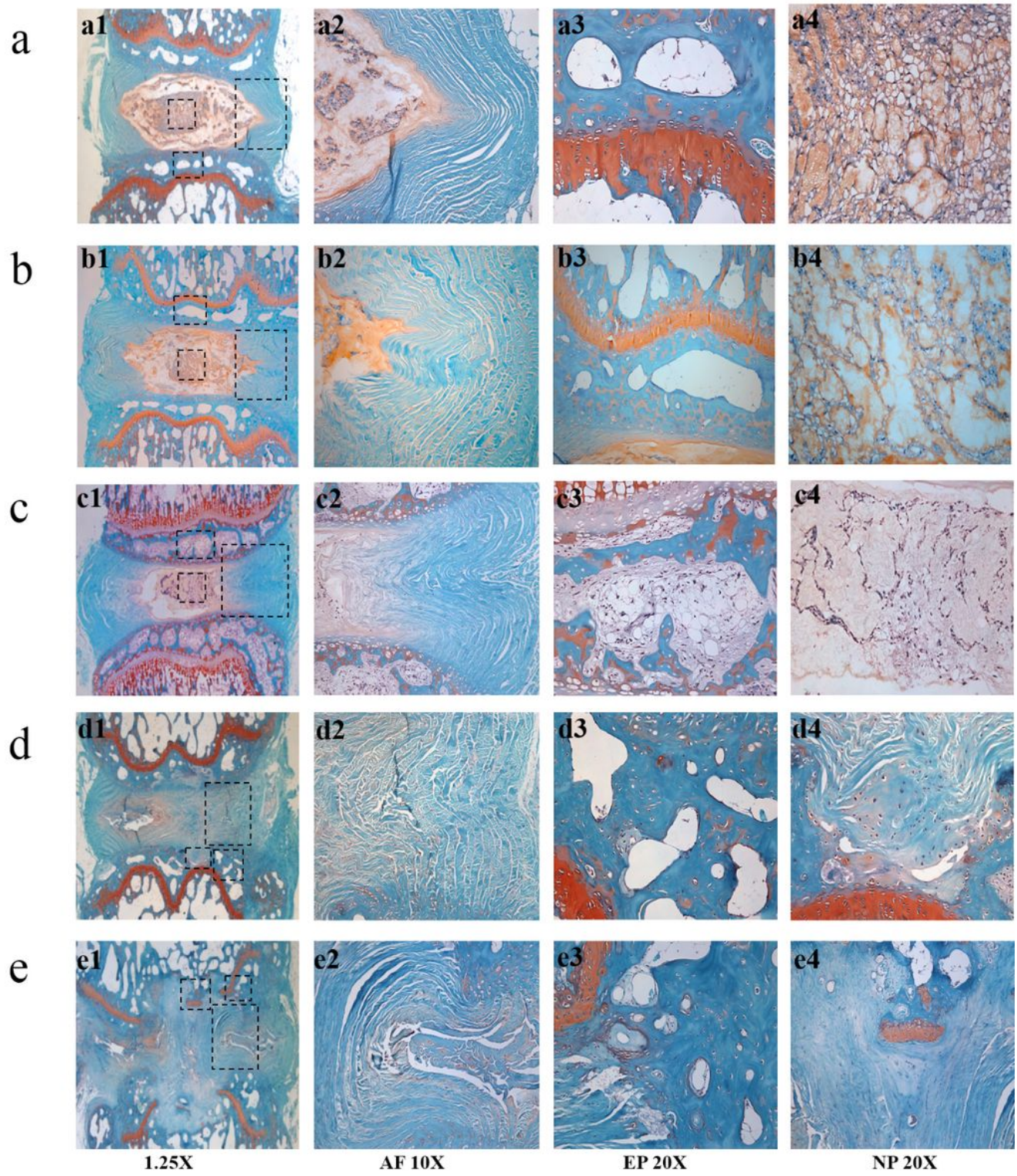

Figure 5

The SOFG stainings of the compressed Co8/9 intervertebral discs in three groups, a. the control group; b. the sham group; c. 1st month after operation; d. 2nd month after operation; e. 3rd month after operation. (a1/b1/c1/d1/e1 indicate the Co8-9 intervertebral disc; a2/b2/c2/d2/e2 indicate AF; a3/b3/c3/d3/e3 indicate CEP; a4/b4/c4/d4/e4 indicate NP; the red arrows show the typical Schmorl's nodule)

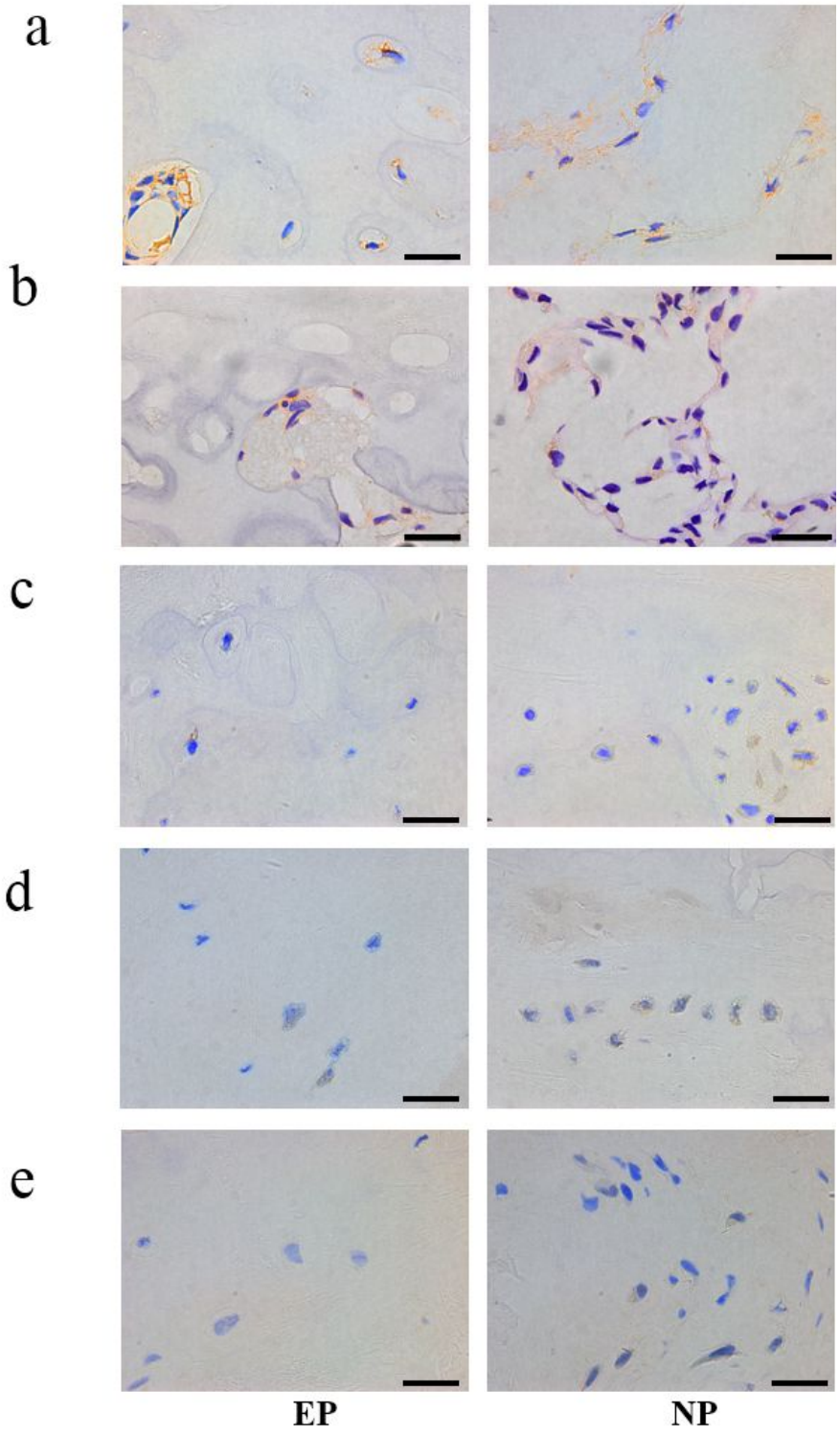

Figure 6

Immunohistochemistrical staining of the matrix aggrecan of Co8-9 intervertebral cartilage endplates and nucleus pulposus cells in three groups, a. the control group; b. the sham group; c. the operational group after loading of 1; d. 2 and e. 3 months. (Bar=20μm, EP= endplate, NP=nucleus pulposus)

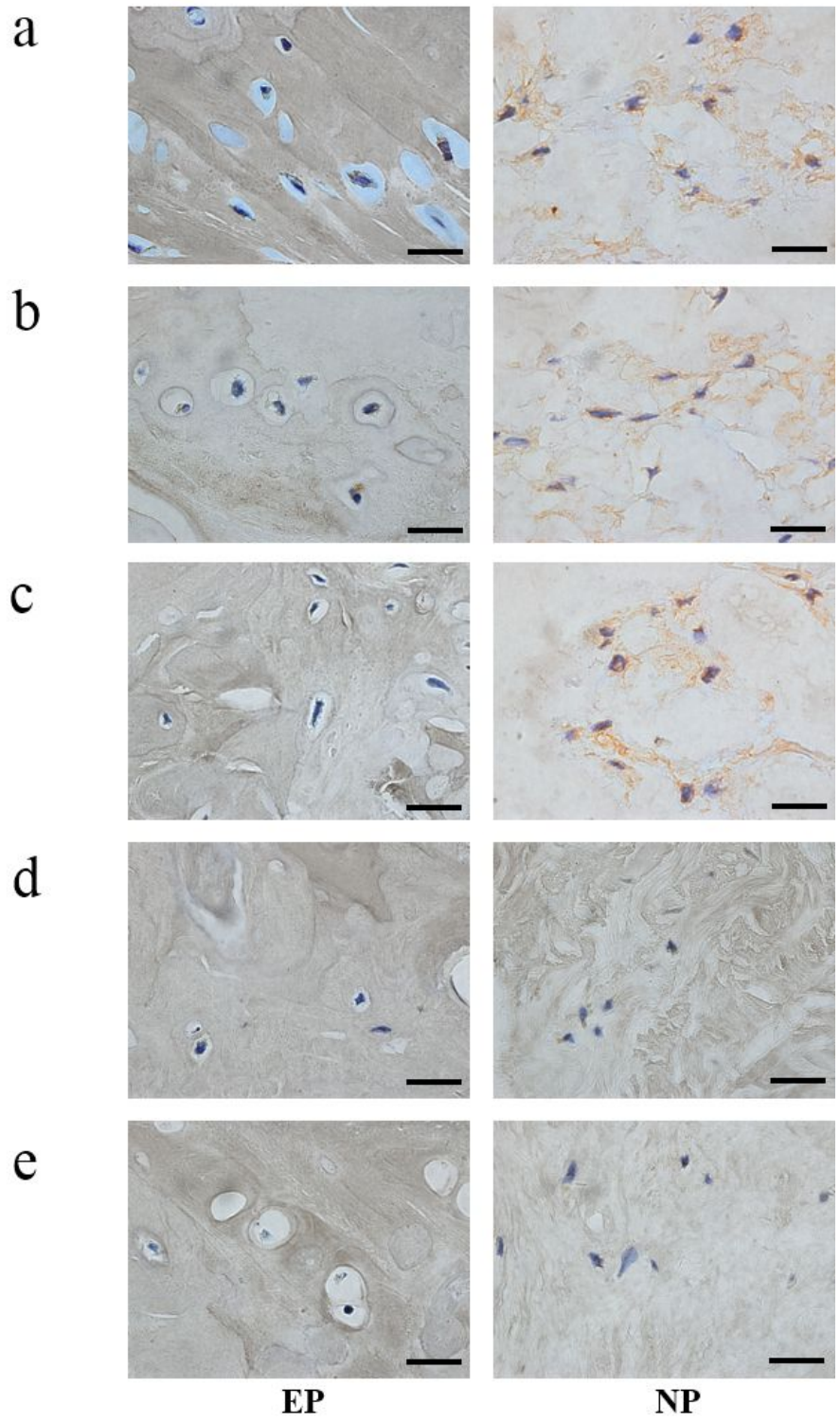

Figure 7

Immunohistochemistrical staining of the matrix collagen II of Co8-9 intervertebral cartilage endplates and nucleus pulposus cells in three groups, a. the control group; b. the sham group; c. the operational group after loading of 1; d. 2 and e. 3 months. (Bar=20μm, EP= endplate, NP=nucleus pulposus)

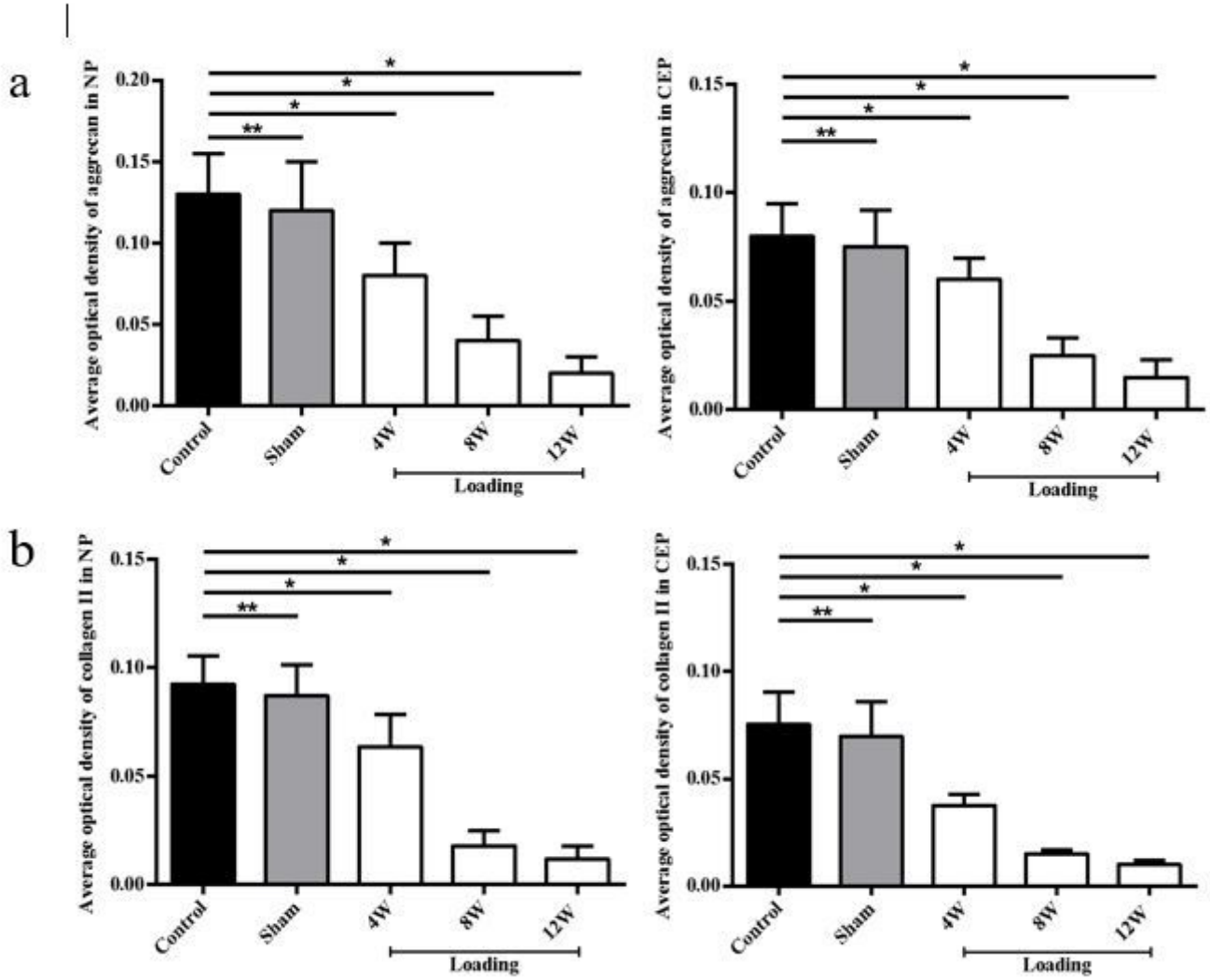

Figure 8

Comparisons of the average optical density values of aggrecan and collagen II in CEP and NP extracellular matrix. (*P<0.05; **P>0.05)

Supplementary Files

This is a list of supplementary files associated with this preprint. Click to download.

- NC3RsARRIVEGuidelinesChecklist2014.docx